

Strangeon Ergostars

Haojia Xia  ¹ Shichuan Chen, ^{1,2} Hong-Bo Li  ^{2,*} Enping Zhou  ^{3,†} and Ren-Xin Xu  ^{4,1,2,‡}

¹*Department of Astronomy, School of Physics, Peking University, Beijing 100871, China*

²*Kavli Institute for Astronomy and Astrophysics, Peking University, Beijing 100871, China*

³*School of Physics, Huazhong University of Science and Technology, Wuhan 430074, China*

⁴*State Key Laboratory of Nuclear Physics and Technology, Peking University, Beijing 100871, China*

(Dated: January 6, 2026)

The nature of the central engine powering short gamma-ray bursts (sGRBs) in binary neutron star (BNS) mergers remains a key open question in the era of multi-messenger astronomy. The ergostar hypothesis, that a rapidly rotating star with an ergoregion drives the relativistic jet, offers an alternative explanation to the black hole-accretion disk paradigm. However, previous studies based on conventional neutron star equations of state (EOSs) have shown that dynamically stable ergostars do not exist unless very extreme EOS or rotation are adopted, casting significant doubt on their astrophysical viability in reality. In this work, however, we examine this hypothesis using a phenomenological EOS of strangeon matter, i.e., condensed matter with nucleon-like units for three flavors of quarks. By constructing a large suite of uniformly rotating equilibrium models, we systematically investigate the parameter space of the stable ergostars and calculate their maximum extractable energy. In contrast to the case of conventional EOSs, we demonstrate that strangeon matter supports a vast and robust parameter space for dynamically stable ergostars, even without requiring differential rotation. We find that the extractable rotational energy from these configurations can be on the order of $0.01M_{\odot}$, a reservoir sufficient to power a typical sGRB. Our results revitalize the ergostar as a viable central engine for sGRB, suggesting that BNS merger remnants composed of exotic matter could play a crucial, previously underestimated role in high-energy astrophysics.

I. INTRODUCTION

Short gamma-ray bursts (sGRB) are among the most violent astrophysical phenomena in the universe. The multi-messenger observation of the binary neutron star (BNS) merger GW170817 provided decisive evidence that such mergers are a primary progenitor of sGRB [1–3]. In the standard paradigm, the central engine is a nascent black hole surrounded by an accretion disk [4]. However, the viability of alternative scenarios—particularly those involving a long-lived, hypermassive neutron star (or magnetar) remnant—remains an open and important question [5–7].

Alternatively, Komissarov [8, 9] proposed that the central engine could be a rapidly rotating compact star containing an ergoregion, often referred to as an ergostar. In general relativity, the ergoregion is a region of spacetime where the stellar rotation is so strong that no particle can remain stationary with respect to a distant observer. Instead, all trajectories, including those of light, are forced to co-rotate with the star. Mathematically, this corresponds to the condition where the metric component $g_{tt} > 0$.

Such extreme frame-dragging allows for the existence of negative-energy states relative to infinity. These states open a physical channel for energy extraction from a BNS merger remnant to power the relativistic jet of an sGRB, analogous to the Penrose process for black holes [10], provided that the ergostar remains stable for a sufficient duration. If the configuration proves unstable, the ergoregion may disappear, or the star may collapse entirely, before the jet is formed.

This stability problem is intrinsically connected to the equation of state (EOS) of dense matter. Numerical results from Tsokaros *et al.* [11] indicate that, for conventional nuclear matter EOSs, dynamically stable ergostars are extremely rare in parameter space and typically require substantial differential rotation.

In fact, the true EOS of supranuclear matter remains still unknown due to the difficulty from ab-initial calculations, but strangeness matters [e.g., 12, 13]. As Witten [14] proposed that the true ground state of dense matter might be quark matter, composed of nearly free u , d , and s quarks, and this idea implies that compact objects resembling pulsars could be strange quark stars (SqSs) rather than traditional neutron stars (NSs), as modeled in the MIT bag model within the asymptotic freedom regime [15]. Can quarks really be asymptotically free there? Could nucleon-like units form due to the non-perturbative nature of the fundamental strong interaction at low energies as in the case of atomic nucleus? Xu [16] suggested then that the building blocks of supranuclear matter could instead be strange quark clusters, termed strangeons, rather than itinerant quarks. This is because the coupling between quarks remains very strong [17]. These strangeons, formed by bound u , d , and s quarks, represent a unique state of matter in which quarks condense in position space rather than momentum space. The term strangeon stars (SnSs) was coined to describe such compact objects [17–20].

Strangeon matter, like strange quark matter, consists of nearly equal numbers of u , d , and s quarks. In contrast to strange quark matter, quarks in strangeon matter are localized inside strangeons due to the strong quark-quark coupling. NSs, SqSs and SnSs have similarities but also differ significantly. In SnSs, quarks are localized in strangeons, much like neutrons in NSs. However, unlike neutrons, a strangeon can contain more than three valence quarks, restoring light-flavour symmetry.

* Corresponding author: lihb2020@pku.edu.cn

† Corresponding author: ezhou@hust.edu.cn

‡ Corresponding author: r.x.xu@pku.edu.cn

SnSs are self-bound by the strong force, with their surface matter also composed of strangeons, similar to SqSs [16].

The SnSs model can account for many key observational phenomena in astrophysics. The EOS of SnSs is sufficiently stiff to explain the observed masses of pulsars [21, 22], while pulsar glitches may be naturally attributed to starquakes [23]. Moreover, SnSs provide a potential explanation for X-ray flares and bursts in magnetar candidates [24], the plateau phase observed in gamma-ray bursts [25], and the quasi-periodic oscillations in SGR 1806–20 [26]. They also help to shape the energy budget of various astrophysical power sources within the framework of magnetar starquake triggering mechanisms [27]. In addition, the strangeness barrier plays a crucial role in understanding Type I X-ray bursters [28], X-ray-dim isolated neutron stars [29, 30], and the nature of the Ultraluminous X-ray sources [31].

In this work, we investigate the dynamic stability of the ergostars based on the SnS model. We utilize the publicly available `rns` code to construct equilibrium sequences of differentially rotating stars and identify ergostar solutions using the $g_{tt} > 0$ criterion. The dynamic stability of these solutions is analyzed via the turning-point method [32]. On this basis, we estimate the maximum extractable rotational energy by calculating the amount of energy loss required for the ergoregion to vanish or for the star to collapse into a black hole. We find that, in contrast to the case of conventional EOSs, strangeon matter supports a robust population of dynamically stable ergostars with an available energy budget ($\sim 10^{52}$ erg) sufficient to power a typical sGRB.

The paper is organized as follows. In Sec. II, we introduce the EOS of SnSs adopted in this work. We discuss in Sec. III the results of our systematic survey, identifying the parameter space for stable ergostars and calculating their maximum extractable energy. Finally, we summarize and discuss our results in Sec. IV.

II. EQUATION OF STATE

As an analogy of the interaction between nucleons, we assume that the interaction potential between two strangeons is parameterized by the Lennard-Jones potential [33–39],

$$U(r) = 4\epsilon \left[\left(\frac{\sigma}{r} \right)^{12} - \left(\frac{\sigma}{r} \right)^6 \right], \quad (1)$$

where r is the distance between two strangeons, ϵ is the depth of the potential well representing the interaction strength, and σ is the characteristic distance scale where the potential is zero.

From this two-body potential, the energy density ρ and pressure P of bulk strangeon matter at zero temperature can be derived by assuming a crystal lattice structure[34]:

$$\begin{aligned} \rho &= 2\epsilon \left(A_{12}\sigma^{12}n^5 - A_6\sigma^6n^3 \right) + nN_qm_q, \\ P &= n^2 \frac{d(\rho/n)}{dn} = 4\epsilon \left(2A_{12}\sigma^{12}n^5 - A_6\sigma^6n^3 \right), \end{aligned} \quad (2)$$

where $A_{12} = 6.2$, $A_6 = 8.4$, n is number density of strangeons, N_q is number of quarks in a strangeon, and m_q is the average constituent quark mass.

The EOS can be recast in terms of two parameters through a normalization procedure. This procedure begins by replacing the microscopic parameter σ with the macroscopic surface baryon number density, $n_{\text{sur}} = (A_6/2A_{12})^{1/2} N_q/3\sigma^3$, the density at which the pressure vanishes. Then, the potential depth ϵ and the number density n are normalized. The normalized potential depth is defined as $\tilde{\epsilon} = \epsilon/N_q$, representing the potential depth contribution per quark, which serves as a measure of interaction strength independent of the strangeon's size. The number density is normalized as \bar{n} , relating the local density to the surface density.

This process yields the final “two-parameter model” form used in our analysis [39]:

$$\frac{\rho}{n_{\text{sur}}} = \frac{a}{9} \tilde{\epsilon} \left(\frac{1}{18} \bar{n}^5 - \bar{n}^3 \right) + m_q \bar{n}, \quad (3)$$

$$\frac{P}{n_{\text{sur}}} = \frac{2a}{9} \tilde{\epsilon} \left(\frac{1}{9} \bar{n}^5 - \bar{n}^3 \right). \quad (4)$$

Here, the normalized number density is $\bar{n} = (N_q n)/n_{\text{sur}}$. The model contains several fixed constants. Following the original paper[37, 39], the number of quarks per strangeon, $N_q = 18$, the parameter a derived from lattice sum constants of the Lennard-Jones potential, is defined as $a = A_6^2/A_{12} = 8.4^2/6.2 \approx 11.38$, the average constituent quark mass m_q is taken to be 300 MeV.

The entire thermodynamic behavior of the strangeon matter is uniquely determined by two free parameters. The first is the normalized potential depth, $\tilde{\epsilon}$ (in MeV), which primarily controls the stiffness of the EOS, a larger $\tilde{\epsilon}$ corresponds to stronger short-range repulsion and thus a stiffer EOS. The second parameter is the surface baryon number density, n_{sur} (in fm^{-3}), which sets the saturation density of the self-bound matter. A lower value of n_{sur} also contributes to a stiffer EOS.

An important feature of this EOS, inherited from its Lennard-Jones potential, is that the adiabatic speed of sound, defined as $c_s^2 = dP/d\rho$, can exceed the speed of light at high densities. This seemingly acausal behavior is a known characteristic of models employing classical, action-at-a-distance potentials [40, 41]. Following the established arguments [34, 41], it is crucial to distinguish this adiabatic sound speed from the true physical signal propagation speed. The value of c_s is derived from the static equilibrium relation and should be interpreted as a measure of the matter's local stiffness. A true physical signal, however, is a dynamic disturbance whose velocity depends on the underlying field theory mediating the interaction. The apparent superluminal nature of c_s in this phenomenological model is a consequence of the idealized, instantaneous interaction assumed in the potential. Therefore, in this work, we treat c_s not as a signal velocity, but purely as a quantitative measure of the EOS stiffness, with the fundamental causality of the underlying strong interaction assumed to be preserved.

To systematically investigate the properties of this EOS, we explore a broader parameter space than that constrained by

the Bayesian analysis of Yuan *et al.* [39]. We select a series of values for $\tilde{\epsilon}$: 0.1, 1.0, and 3.0 MeV. These values represent scenarios that are, respectively, much softer, slightly stiffer, and significantly stiffer than the observationally favored results. For each value of $\tilde{\epsilon}$, we generate a set of EOSs by uniformly sampling 30 points for n_{sur} within the range of $(0.1, 0.36) \text{ fm}^{-3}$.

III. RESULTS

A. Overview of Ergostar Analysis

To investigate the properties of ergostars, we perform a systematic analysis for the EOS model. Our equilibrium models of rotating compact stars are constructed using the publicly available `rns` code [42]. This code solves the Einstein field equations for a stationary and axisymmetric spacetime, whose metric is given by

$$ds^2 = -e^{\gamma+\beta} dt^2 + e^{2\alpha} (dr^2 + r^2 d\theta^2) + e^{\gamma-\beta} r^2 \sin^2 \theta (d\phi - \omega dt)^2, \quad (5)$$

where γ , β , α , and the frame dragging frequency ω are functions of the coordinates r and θ . The energy-momentum tensor is given by

$$T^{\mu\nu} = (\rho + P)u^\mu u^\nu + Pg^{\mu\nu}, \quad (6)$$

where P is the pressure and ρ is the energy density. In this work, we employ the phenomenological strangeon EOS, the details and parameterizations of which are presented in Sec. II.

A crucial assumption in our framework is that the stars are in rigid (uniform) rotation, meaning the angular velocity Ω is constant throughout the star. This allows us to isolate the effects of the EOS on ergostar formation, in contrast to previous studies that often required strong differential rotation [11]. The computational procedure is as follows: for a given EOS, we generate a sequence of equilibrium solutions by incrementally increasing the central baryon density, ρ_c . For each resulting stellar model, we then test for the existence of an ergoregion by evaluating the sign of g_{tt} across the stellar interior. An ergoregion is identified where the following condition is satisfied:

$$g_{tt} = -e^{\gamma+\beta} + e^{\gamma-\beta} r^2 \sin^2 \theta \omega^2 > 0. \quad (7)$$

For each EOS, the analysis proceeds via a two-dimensional parameter space scan over the angular momentum J and central baryon density ρ_c . We map the resulting equilibrium solutions onto the gravitational mass–central density ($M-\rho_c$) plane. In this plane, the domain of dynamically stable ergostars is delineated by the intersection of two physical conditions. First, the solution must satisfy the condition $g_{tt} > 0$ (Eq. 7) to possess an ergoregion. Second, the solution must lie on the stable branch of the equilibrium sequence, defined by the turning-point criterion [32]. Based on this domain, we isolate the stable ergostar population and identify two critical boundary solutions: the stable ergostar with the minimum gravitational

mass ($M_{\text{min-ergo}}$) and the one with the maximum gravitational mass ($M_{\text{max-ergo}}$).

After projecting these stable solutions onto the angular momentum–mass ($J-M$) plane, the stable ergostar solutions are strictly confined between the points corresponding to $M_{\text{min-ergo}}$ and $M_{\text{max-ergo}}$. This feature provides a practical diagnostic for astrophysical viability. By overlaying this stable ergostar region with the specific $J-M$ relation imposed by the BNS merger process—specifically the angular momentum budget of the remnant—one can rapidly assess whether a specific EOS is capable of supporting stable ergostars consistent with post-merger conditions.

B. Scaling Relations of Ergostar Solutions

A key feature of the strangeon EOS is the presence of simple scaling relations with respect to the surface baryon density, n_{sur} . For a fixed potential depth per quark, $\tilde{\epsilon}$, this manifests as a strong linear correlation between the macroscopic properties (e.g., mass and angular momentum) of stellar models computed for different values of n_{sur} , as explicitly demonstrated in Figs. 1, 2, and 3. This scaling behavior provides a powerful computational advantage, significantly simplifying the exploration of the parameter space. It allows us to efficiently map the properties across the full range of n_{sur} and accurately identify the regions of interest for our subsequent analysis on ergostar formation.

Upon examining these scaling relations, a notable distinction emerges. For the central densities (Fig. 1) and gravitational masses (Fig. 2), the linear fits are remarkably similar across the different $\tilde{\epsilon}$ families. The slopes of the best-fit lines exhibit only a very weak dependence on $\tilde{\epsilon}$, resulting in the three dashed lines being nearly coincident. This suggests that the properties of the minimum-mass stable ergostar scale in a nearly universal manner with the properties of the maximum-mass spherical star, largely independent of the EOS stiffness.

In stark contrast, the scaling relation for the angular momentum (Fig. 3) demonstrates a strong and systematic dependence on $\tilde{\epsilon}$. The slope of the linear fit decreases monotonically as $\tilde{\epsilon}$ increases, with values of 0.62, 0.51, and 0.46 for $\tilde{\epsilon} = 0.1, 1$, and 3 MeV, respectively. This trend has a direct physical interpretation that is qualitatively visible in the $J-M$ plane (Fig. 4). A smaller slope in the $J_{\text{min-ergo}}-J_{\text{max-ergo}}$ relation implies a larger vertical separation between the lower and upper boundaries of the stable ergostar domain in the $J-M$ plane. Physically, this signifies that a stiffer EOS (larger $\tilde{\epsilon}$) supports a wider range of angular momenta over which stable ergostars can exist.

To connect these theoretical models to the astrophysical outcomes of BNS mergers, we employ the empirical relation derived by Bauswein and Stergioulas [43]. The empirical relation between angular momentum of the remnant and the total binary mass is largely insensitive to the underlying EOSs:

$$J_{\text{merger}} \simeq a M_{\text{tot}} - b, \quad (8)$$

where J_{merger} is the angular momentum of merger remnant, M_{tot} is total binary mass, and the fitting constants are $a = 4.041$ and $b = 4.658$. To apply this relation, we adopt the common

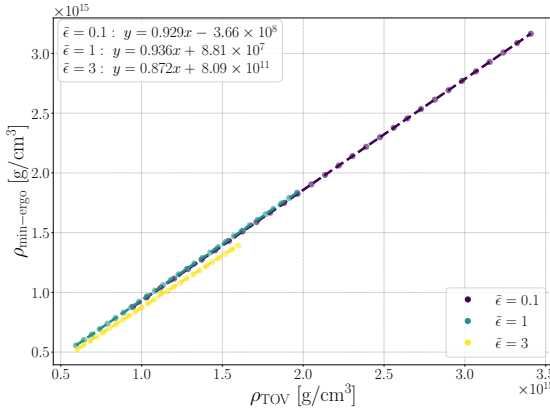


FIG. 1. Scaling relation between the central density of the minimum-mass stable ergostar ($\rho_{c,\text{min-ergo}}$) and the central density of the maximum spherical mass ($\rho_{c,\text{TOV}}$) for each EOS parameter set. Each color corresponds to a different fixed value of the potential depth per quark, $\tilde{\epsilon}$. The solid points denote individual parameter combinations from our systematic survey, while the dashed lines represent the linear fits for each family of models. The best-fit formulas are displayed in the plot.

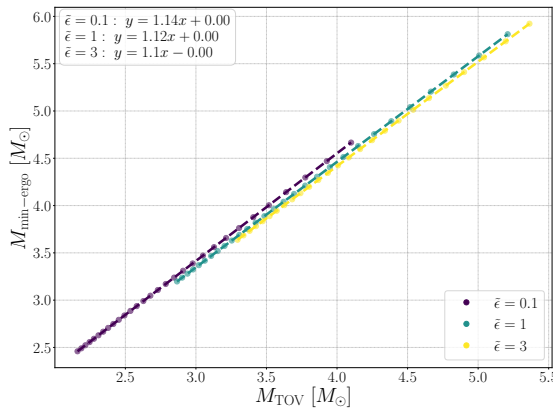


FIG. 2. Scaling relation between the gravitational mass of the minimum-mass stable ergostar ($M_{\text{min-ergo}}$) and the maximum spherical (TOV) mass (M_{TOV}). As in the previous figure, each color corresponds to a fixed value of $\tilde{\epsilon}$. The solid points represent individual parameter combinations, and the dashed lines are their respective linear fits. The fitting formulas are shown in the plot.

approximation that the gravitational mass of the remnant is equal to the total binary mass ($M_{\text{remnant}} \approx M_{\text{tot}}$), neglecting the small percentage of mass lost during the merger process. A case of EOS is considered a viable candidate for forming a transient ergostar remnant only if its region of ergostar existence straddles this empirical line. As illustrated in Fig. 4, this criterion allows us to narrow down the set of physically interesting cases significantly.

Among all the feasible candidate models, we pay special attention to the parameters corresponding to the “Case 4” in the Bayesian analysis by Yuan *et al.* [39]. This particular case, with $\tilde{\epsilon} = 0.61 \text{ MeV}$ and $n_{\text{sur}} = 0.18 \text{ fm}^{-3}$, is highly compelling because it is constrained by the most comprehen-

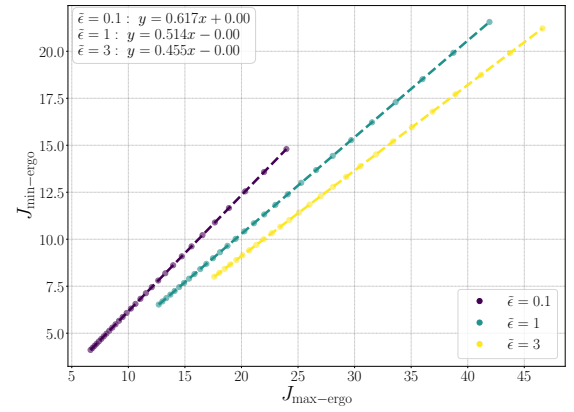


FIG. 3. Scaling relation between the angular momentum of the minimum-mass stable ergostar ($J_{\text{min-ergo}}$) and the angular momentum of the maximum-mass stable ergostar ($J_{\text{max-ergo}}$). The legend follows that of the previous figures: points are grouped by color according to their $\tilde{\epsilon}$ value, and the dashed lines represent the corresponding linear fits.

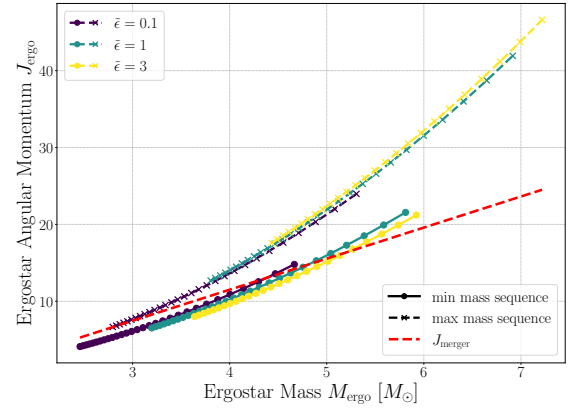


FIG. 4. The total angular momentum as functions of the gravitational mass with different parameters. For each value of $\tilde{\epsilon}$, the solid lines with filled circles and the dashed lines with crosses represent the sequences of minimum and maximum mass ergostars, respectively. The red dashed line represents the empirical threshold for prompt collapse from Bauswein and Stergioulas [43].

sive set of multi-messenger observations, incorporating data from NICER pulsars [44–49] as well as the gravitational-wave events GW170817 [1] and GW190814[50].

At fixed angular momenta, we analyze this scenario by first calculating sequences of rotating solutions for the SnS model. For each sequence, solutions with varying central densities are generated and plotted on an $M-\rho_c$ diagram (see Fig. 5). Moreover, for each sequence of constant angular momentum, we plot the turning point of the maximum mass, which is indicated by the maximum mass marks the onset of secular instability [32].

Although the onset of dynamical instability occurs at a slightly lower central density, extensive studies have demonstrated that the loci of secular and dynamical instabilities are nearly coincident [43, 51]. Given the close proximity of these critical points, we adopt the turning-point line as a practical

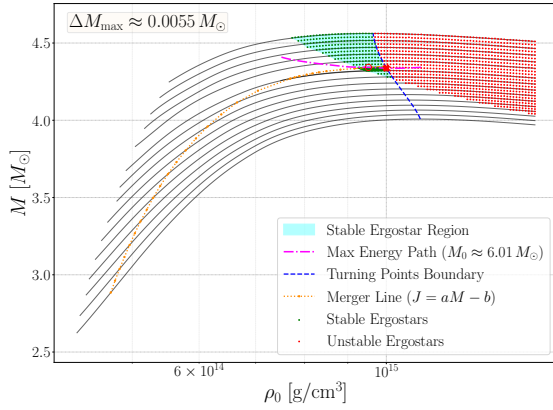


FIG. 5. The gravitational mass versus the central density of SnS. Sequences of constant angular momentum are shown as black solid lines. Their turning points, which define the stability limit, are connected by the blue dashed line. Dynamically stable and unstable solutions are marked by green and red solid circles, respectively. The cyan region highlights the inferred domain of stable ergostars. Also shown are the empirical line for merger remnants (orange dashed) and the path of maximum energy extraction (purple dashed), which starts at the red circle and terminates at the red cross. The total energy released along this path is $0.0055 M_{\odot}$.

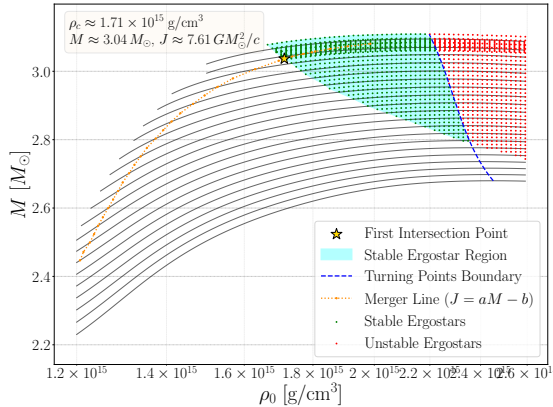


FIG. 6. Gravitational mass versus central density for a strangeon star with EOS parameters $\bar{\epsilon} = 0.3$ MeV and $n_{\text{sur}} = 0.36$ fm $^{-3}$. This represents the softest EOS within the Yuan *et al.* [39] parameter space that can form a post-merger ergostar. Sequences of constant angular momentum are shown as black solid lines, with their turning points (the stability limit) connected by the blue dashed line. Dynamically stable and unstable solutions are marked by green and red solid circles, respectively. The cyan region highlights the inferred domain of stable ergostars. The orange dashed line is the empirical relation for merger remnants. The gold star marks the first intersection point between the merger remnant line and the stable ergostar domain, representing the minimum-mass dynamically stable ergostar that can be formed from a BNS merger for this EOS. The gravitational mass, central density, and angular momentum of this minimum-mass configuration are listed in the top-left corner.

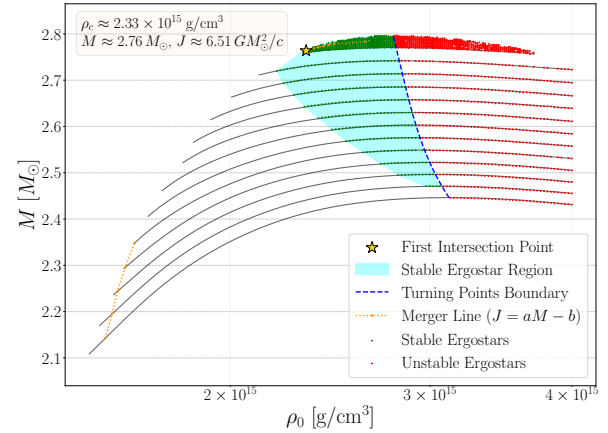


FIG. 7. Same as Fig. 6, but for EOS parameters $\bar{\epsilon} = 0.1$ MeV and $n_{\text{sur}} = 0.36$ fm $^{-3}$. This configuration corresponds to the minimum-mass ergostar remnant found in our extended parameter survey. The gold star again marks this minimum-mass configuration, with its properties listed in the top-left corner.

criterion to delineate the boundary of the dynamically stable region for our ergostar solutions. This approach allows us to systematically map the domain of stable configurations in the M – ρ_c plane. We further identify an empirical line corresponding to the merger remnants [43], which serves as a reference for subsequent analysis.

C. Extractable Energy

Building on this stability scenario, we hypothesize an energy-extraction process that proceeds along a sequence of constant baryon mass. Each evolutionary path begins from a configuration located below the merger-remnant line and terminates at the point of minimum gravitational mass along that sequence, provided it remains within the stable ergostar region. The released energy for a given path is then evaluated as

$$\Delta E = M_{\text{initial}} - M_{\text{final}}. \quad (9)$$

This method enables us to identify the trajectory that maximizes the energy release and to quantify its value. Applying this framework to a representative case, we find that stable ergostars can indeed form beneath the merger-remnant line [43], releasing up to $0.0055 M_{\odot}$ in extractable energy, as illustrated in Fig. 5.

A question of significant astrophysical interest is determining the minimum mass required for a BNS merger to produce a transient ergostar remnant within our framework. In general, for any given parameter space, provided that an intersection between the empirical J – M relation and the domain of stable ergostar solutions exists, the minimum-mass ergostar that can be formed will correspond to the softest possible EOS.

Applying this principle to the parameter space chosen by Yuan *et al.* [39] ($\bar{\epsilon} \in (0.3, 3)$ MeV and $n_{\text{sur}} \in (0.17, 0.36)$ fm $^{-3}$), we find that the softest EOS that still permits the formation of

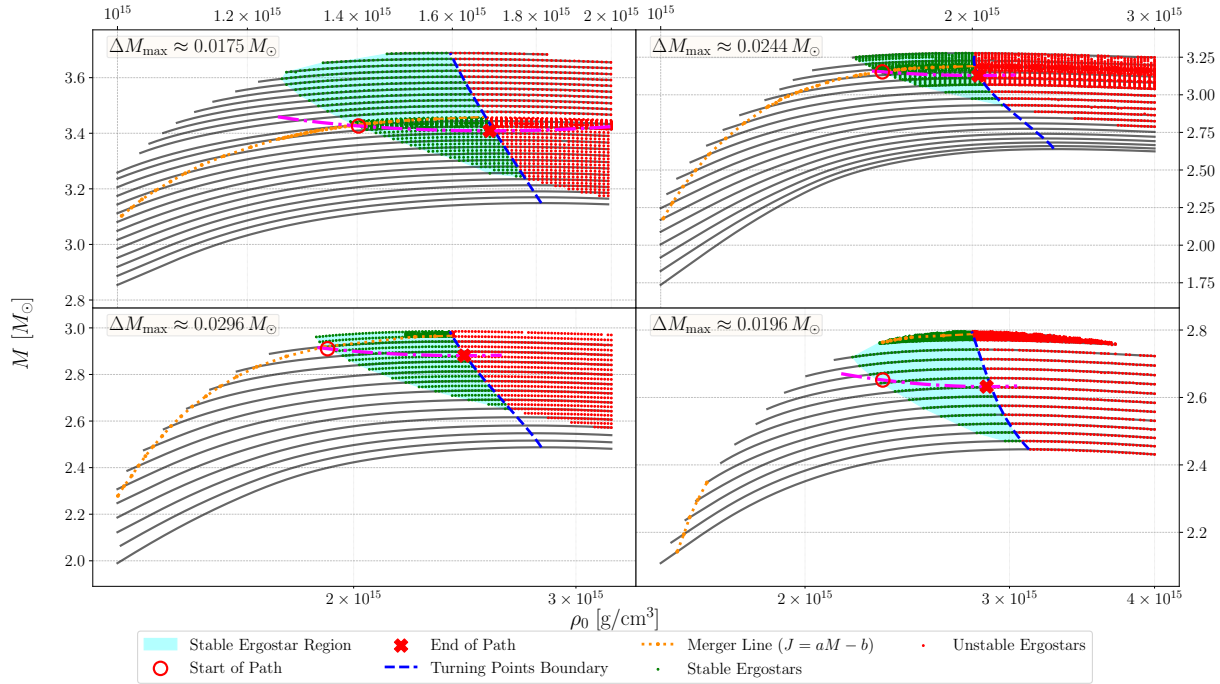


FIG. 8. Ergostar solutions for the strangeon matter EOS with a fixed potential depth per quark of $\tilde{\epsilon} = 0.1$ MeV. The four panels correspond to different values for the surface baryon density, n_{sur} : the top left, top right, bottom left, and bottom right panels show the cases for $n_{\text{sur}} = 0.2061, 0.2539, 0.3069$, and 0.36 fm^{-3} , respectively. In each panel, the graphical elements are defined as follows. The black solid lines are sequences of constant angular momentum, the blue dashed line connects their turning points; green and red solid circles mark dynamically stable and unstable solutions, the light blue region shows the inferred stable domain, the orange dashed line is the empirical relation for merger remnants from Eq. (8), and the purple dashed line indicates the path of maximum energy extraction. The maximum extractable energy for each case, denoted as ΔM_{max} , is explicitly labeled within each panel.

a merger remnant occurs at the boundary where $\tilde{\epsilon} = 0.3$ MeV and $n_{\text{sur}} = 0.36 \text{ fm}^{-3}$. As shown in Fig. 6, the resulting minimum-mass ergostar remnant has a gravitational mass of $3.04 M_{\odot}$, a central density of $1.71 \times 10^{15} \text{ g cm}^{-3}$, and an angular momentum of $7.61 GM_{\odot}^2/c$.

If we extend the lower bound of $\tilde{\epsilon}$ to 0.1 MeV, the new minimum is found at $\tilde{\epsilon} = 0.1$ MeV and $n_{\text{sur}} = 0.36 \text{ fm}^{-3}$ (see Fig. 7). This configuration yields an ergostar with a mass of $2.76 M_{\odot}$, a central density of $2.33 \times 10^{15} \text{ g cm}^{-3}$, and an angular momentum of $6.51 GM_{\odot}^2/c$.

Beyond the case 4, we conduct a systematic parameter survey to examine how the EOS parameters affect both ergostar stability and energy extraction. In Sec. III B, we have identified a pool of viable candidate models in which the domain of stable ergostar configurations intersects the empirical merger-remnant line in the J – M plane. From this pool, we select a representative subset of twelve models for detailed investigation. These models are grouped according to the potential depth per quark, $\tilde{\epsilon} = 0.1, 1$, and 3 MeV, allowing us to systematically probe the behavior of soft, intermediate, and stiff EOSs. Within each group, four distinct surface baryon densities, n_{sur} , are considered.

The key properties of these twelve representative models—including the maximum spherical mass (M_{TOV}) and the corresponding central density ($\rho_{c,\text{TOV}}$)—are summarized in Table I. The table also lists the principal result for each case:

the maximum extractable energy, ΔM_{max} .

In Fig. 8, we show the relations between the mass and the central density for SnS with $\tilde{\epsilon} = 0.1$. We find a clear trend for the first three values of n_{sur} and the maximum extractable mass, ΔM_{max} , increases from 0.0175, through 0.0244, to 0.0296 M_{\odot} as n_{sur} is increased from 0.2061 to 0.3069 fm^{-3} . This behavior can be traced to the evolving geometry between the empirical merger-remnant line and the region of dynamically stable ergostar configurations. Furthermore, as n_{sur} increases within this interval, the vertical separation between these two loci in the M – R plane widens, enabling a longer path for the energy-extraction sequence along a line of constant baryon mass. The extended path length, in turn, translates into a larger amount of released energy.

Of particular interest is the scenario presented in the bottom-right panel of Fig. 8 ($n_{\text{sur}} = 0.36 \text{ fm}^{-3}$), which offers a remarkably consistent picture with the multimessenger event GW170817 [1–3]. In this case, the intersection of the stable ergostar domain and the empirical merger-remnant line indicates that a BNS merger can naturally result in a dynamically stable ergostar remnant with a gravitational mass of $M \approx 2.6 M_{\odot}$. Our calculations show that such a remnant allows for an extractable energy budget of approximately $\Delta E \sim 0.02 M_{\odot} c^2$ before it loses sufficient angular momentum to collapse into a black hole. Crucially, we emphasize that this specific strangeon EOS model is fully compatible with existing observational

TABLE I. Properties of selected cases and the corresponding maximum extractable energy from their ergostar remnants. Columns show the identifier, EOS parameters ($\tilde{\epsilon}$ and n_{sur}) [39], the maximum Tolman-Oppenheimer-Volkoff limit (M_{TOV}), its central density ($\rho_{c,\text{TOV}}$), and the calculated maximum extractable energy (ΔE_{max}).

case ID	$\tilde{\epsilon}$ MeV	n_{sur} fm^{-3}	M_{TOV} M_{\odot}	$\rho_{c,\text{TOV}}$ g cm^{-3}	ΔE_{max} M_{\odot}
case A	0.1	0.2061	2.6877	2.23×10^{15}	0.0175
case B	0.1	0.2539	2.5729	2.43×10^{15}	0.0244
case C	0.1	0.3069	2.3400	2.94×10^{15}	0.0296
case D	0.1	0.3600	2.1607	3.45×10^{15}	0.0196
case E	1.0	0.2061	3.7876	1.11×10^{15}	0.0079
case F	1.0	0.2539	3.4128	1.37×10^{15}	0.0234
case G	1.0	0.3069	3.1039	1.66×10^{15}	0.0307
case H	1.0	0.3600	2.8660	1.95×10^{15}	0.0447
case I	3.0	0.2061	4.3558	8.89×10^{14}	0.0087
case J	3.0	0.2539	3.9248	1.10×10^{15}	0.0283
case K	3.0	0.3069	3.5695	1.32×10^{15}	0.0451
case L	3.0	0.3600	3.2960	1.55×10^{15}	0.0513

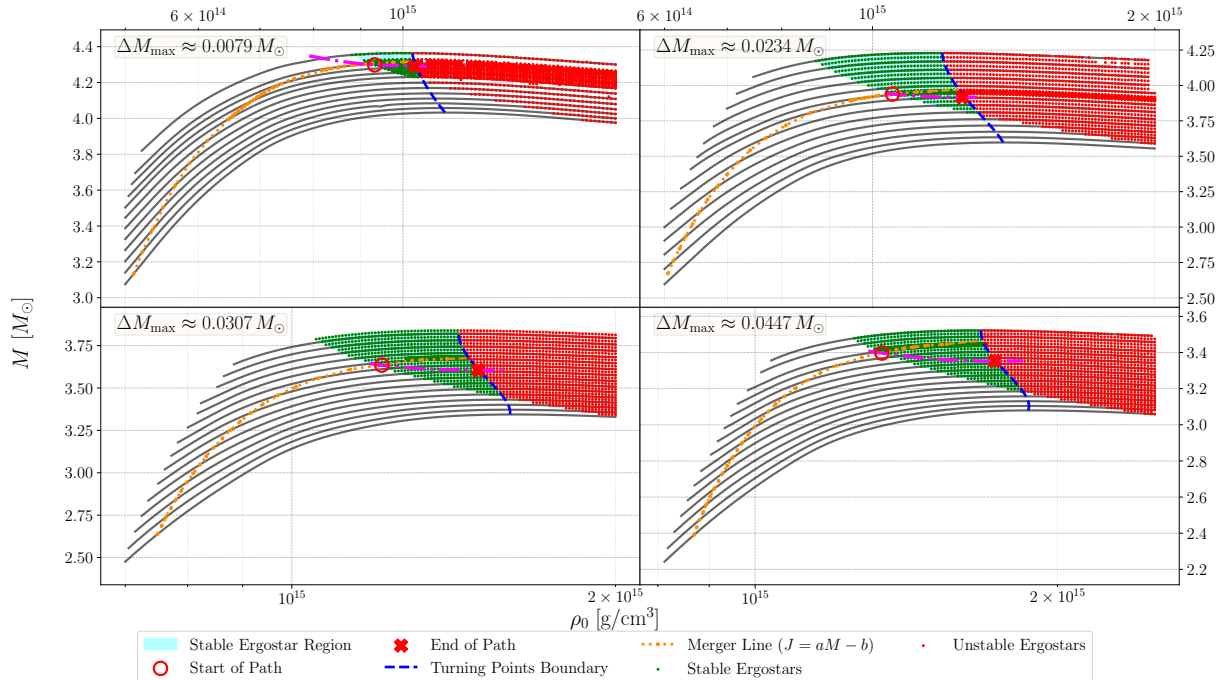


FIG. 9. Same as Fig. 8, but for models with $\tilde{\epsilon} = 1$ MeV. The four panels show results for the same values of n_{sur} in the same arrangement.

constraints, satisfying both the maximum mass requirement ($M_{\text{TOV}} \gtrsim 2M_{\odot}$) and the tidal deformability limits inferred from GW170817 [1–3]. This result completes the logical hierarchy of our investigation: it demonstrates that strangeon matter not only supports dynamically stable ergostars in principle, but specifically allows for the natural formation of such objects within the mass range and physical conditions characteristic of GW170817-like events [1–3].

When comparing the results across different values of $\tilde{\epsilon}$, a general pattern emerges: a larger $\tilde{\epsilon}$, corresponding to a stiffer EOS, generally expands the parameter space for stable ergostars and thus allows for greater energy extraction. However, this relationship is not absolute. A notable excep-

tion occurs at the lowest surface density, $n_{\text{sur}} = 0.2061 \text{ fm}^{-3}$. Counterintuitively, the softest EOS ($\tilde{\epsilon} = 0.1$) yields a larger extractable energy than both the intermediate ($\tilde{\epsilon} = 1, 0.0079 M_{\odot}$) and stiff ($\tilde{\epsilon} = 3, 0.0087 M_{\odot}$) models. This highlights that the potential for energy release is not dictated solely by the overall stiffness of the EOS, but rather by the specific and sometimes non-trivial interplay between the stability boundary and the constraint imposed by the empirical merger line.

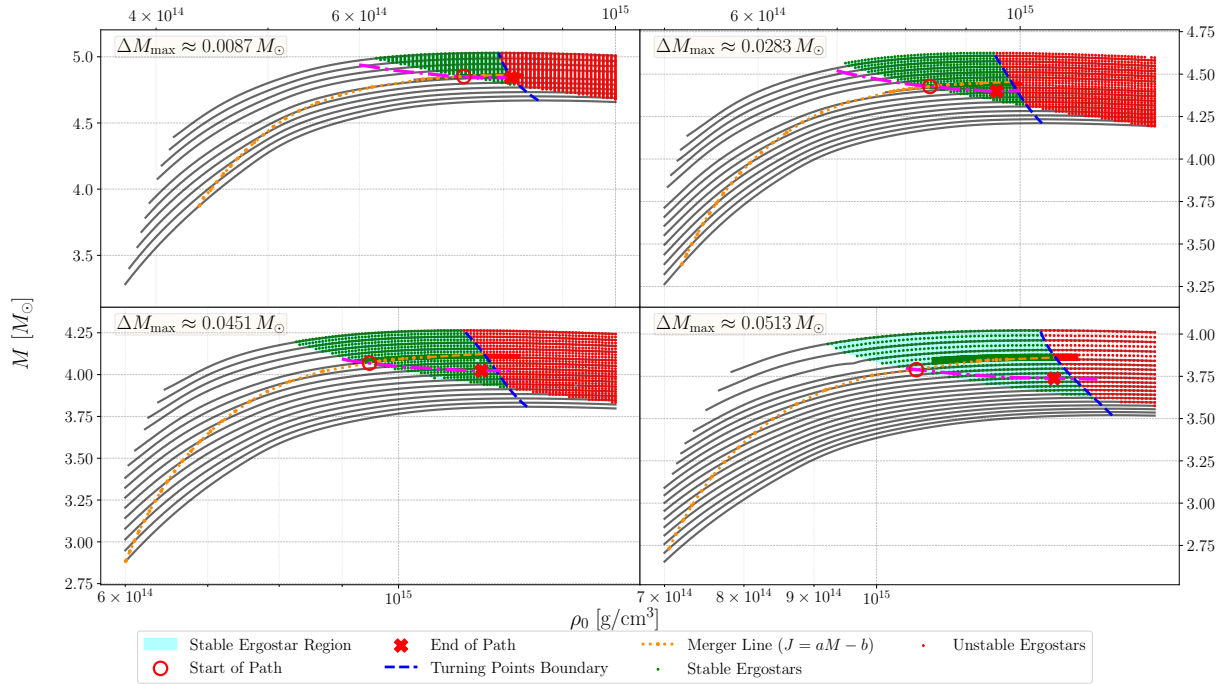


FIG. 10. Same as Fig. 8, but for models with $\epsilon = 3$ MeV, corresponding to a stiffer EOS. The arrangement of the panels remains the same.

IV. DISCUSSION

We have explored the parameter space of dynamically stable ergostars with SnS EOS. In particular, we investigated the possibility of dynamically stable ergostar remnant that could be formed during BNS mergers and the maximum extractable energy from them. A key finding of this work is that the formation of a dynamically stable, uniformly rotating ergostar as a merger remnant is a robust outcome for a wide range of strangeon matter EOS parameters. This stands in notable contrast to previous studies of conventional EOSs, which have generally found that the formation of stable ergostars is challenging, often requiring significant differential rotation or strong magnetic fields to support such configurations [52–54]. Our analysis demonstrates that, for strangeon matter, the post-merger remnant can indeed settle into a transient ergostar state capable of releasing significant energy. While the energy extraction potential depends intricately on the geometry of the domain of stable ergostar solutions, a crucial result is that nearly all models we considered can release energy on the order of $0.01M_\odot$. This represents a substantial energy reservoir, potentially sufficient to power the central engine of a large-scale sGRB or its associated extended emission.

A crucial avenue for future work lies in modeling the specific multi-messenger signatures of the energy release mechanism we have identified. The injection of approximately 10^{52} erg of hydrodynamical energy into the post-merger environment would inevitably leave a distinct imprint on both gravitational wave and electromagnetic observations.

From the perspective of gravitational waves, the energy extraction process would alter the dynamical evolution of the transient remnant, potentially modifying the frequency, duration, and eventual ringdown of the post-merger GW signal. While challenging to detect with current instruments, these signatures are a prime target for next-generation observatories like the Einstein Telescope and Cosmic Explorer, offering a future path to directly probe the remnant's internal processes.

Last but not least, it is urgent to find solid evidence for long-lived remnants from BNS mergers through multi-band electromagnetic observations in order to test the presented ideas, since the maximum mass of SnS, M_{TOV} , could be as high as $\sim 3M_\odot$. The mass of isolated neutron stars is mostly concentrated at $1.4M_\odot$, and it is natural to expect a long-lived SnS after merger, with a mass of $\sim 2.6M_\odot$ if the initial masses are both $\sim 1.4M_\odot$, or with a mass of $\sim 2.7M_\odot$ if $\sim 1.45M_\odot$. In fact, X-ray observation appears consistent with energy injection by a long-lived $\sim 2.6M_\odot$ -central engine for GW 170817 [55], and recently, a BNS merger-relevant scenario involving a long-lived $\sim 2.7M_\odot$ -magnetar has also been suggested for the kilonova of GW 231109/235456 [56].

V. ACKNOWLEDGEMENTS

This work was supported by the China Postdoctoral Science Foundation (2024M760081), the National Natural Science Foundation of China (12447148), and the National SKA Program of China (2020SKA0120100). E. Z. is supported by NSFC Grant No. 12203017 and the National SKA Program of China No. 2020SKA0120300.

[1] B. P. Abbott *et al.* (LIGO Scientific Collaboration and Virgo Collaboration), *Phys. Rev. Lett.* **119**, 161101 (2017).

[2] V. Savchenko, C. Ferrigno, E. Kuulkers, A. Bazzano, E. Bozzo, S. Brandt, J. Chenevez, T. J.-L. Courvoisier, R. Diehl, A. Domingo, L. Hanlon, E. Jourdain, A. von Kienlin, P. Laurent, F. Lebrun, A. Lutovinov, A. Martin-Carrillo, S. Mereghetti, L. Natalucci, J. Rodi, J.-P. Roques, R. Sunyaev, and P. Ubertini, *The Astrophysical Journal Letters* **848**, L15 (2017).

[3] V. Savchenko, S. Mereghetti, C. Ferrigno, E. Kuulkers, A. Bazzano, E. Bozzo, T. J. L. Courvoisier, S. Brandt, R. Diehl, and L. Hanlon, (2017).

[4] R. D. Blandford and R. L. Znajek, *Monthly Notices of the Royal Astronomical Society* **179**, 433 (1977), <https://academic.oup.com/mnras/article-pdf/179/3/433/9333653/mnras179-0433.pdf>.

[5] Z. G. Dai and T. Lu, *Physical Review Letters* **81**, 4301–4304 (1998).

[6] B. Zhang and P. Mészáros, *The Astrophysical Journal* **552**, L35–L38 (2001).

[7] H.-J. Lü, B. Zhang, W.-H. Lei, Y. Li, and P. D. Lasky, *The Astrophysical Journal* **805**, 89 (2015).

[8] S. S. Komissarov, *Monthly Notices of the Royal Astronomical Society* **350**, 427–448 (2004).

[9] S. S. Komissarov, *Monthly Notices of the Royal Astronomical Society* **359**, 801–808 (2005).

[10] R. Penrose, *General Relativity and Gravitation* **7**, 1141 (2002).

[11] A. Tsokaros, M. Ruiz, and S. L. Shapiro, *Physical Review D* **101** (2020), 10.1103/physrevd.101.064069.

[12] X. Lai, C. Xia, and R. Xu, *Advances in Physics X* **8**, 2137433 (2023), arXiv:2210.01501 [hep-ph].

[13] C. Xia, X. Lai, and R. Xu, *arXiv e-prints* , arXiv:2511.01146 (2025), arXiv:2511.01146 [astro-ph.HE].

[14] E. Witten, *Phys. Rev. D* **30**, 272 (1984).

[15] C. Alcock, E. Farhi, and A. Olinto, *ApJ* **310**, 261 (1986).

[16] R.-X. Xu, *ApJ* **596**, L59 (2003), arXiv:astro-ph/0302165.

[17] X. Y. Lai and R. X. Xu, *J. Phys. Conf. Ser.* **861**, 012027 (2017), arXiv:1701.08463 [astro-ph.HE].

[18] R. X. Xu and Y. J. Guo, in *11th Rencontres du Vietnam: Hot Topics in General Relativity and Gravitation* (2017) pp. 119–146, arXiv:1601.05607 [astro-ph.HE].

[19] H.-B. Li, Y. Gao, L. Shao, R.-X. Xu, and R. Xu, *MNRAS* **516**, 6172 (2022), arXiv:2206.09407 [gr-qc].

[20] W.-L. Yuan, C. Huang, C. Zhang, E. Zhou, and R. Xu, *PRD* **111**, 063033 (2025), arXiv:2411.14938 [astro-ph.HE].

[21] P. Demorest, T. Pennucci, S. Ransom, M. Roberts, and J. Hessels, *Nature* **467**, 1081 (2010), arXiv:1010.5788 [astro-ph.HE].

[22] J. Antoniadis *et al.*, *Science* **340**, 6131 (2013), arXiv:1304.6875 [astro-ph.HE].

[23] E. P. Zhou, J. G. Lu, H. Tong, and R. X. Xu, *MNRAS* **443**, 2705 (2014), arXiv:1404.2793 [astro-ph.HE].

[24] R.-X. Xu, D. J. Tao, and Y. Yang, *MNRAS* **373**, L85 (2006), arXiv:astro-ph/0607106.

[25] S. Dai, L. Li, and R. Xu, *Science China Physics, Mechanics, and Astronomy* **54**, 1541 (2011), arXiv:1008.2568 [astro-ph.HE].

[26] H.-B. Li, Y. Kang, Z. Hu, L. Shao, C.-J. Xia, and R.-X. Xu, *MNRAS* **527**, 855 (2023), arXiv:2309.09847 [astro-ph.HE].

[27] W.-Y. Wang, C. Zhang, E. Zhou, X. Liu, J. Niu, Z. Zhou, H. Gao, J. Liu, R. Xu, and B. Zhang, *RAA* **24**, 105012 (2024), arXiv:2405.07152 [astro-ph.HE].

[28] Z. Li, Z. Qu, L. Chen, Y. Guo, J. Qu, and R. Xu, *ApJ* **798**, 56 (2015), arXiv:1405.3438 [astro-ph.HE].

[29] W. Wang, J. Lu, H. Tong, M. Ge, Z. Li, Y. Men, and R. Xu, *ApJ* **837**, 81 (2017), arXiv:1603.08288 [astro-ph.HE].

[30] W.-Y. Wang, Y. Feng, X.-Y. Lai, Y.-Y. Li, J.-G. Lu, X. Chen, and R.-X. Xu, *RAA* **18**, 082 (2018), arXiv:1705.03763 [astro-ph.HE].

[31] H.-B. Li, S.-J. Gao, X.-D. Li, and R.-X. Xu, *arXiv e-prints* , arXiv:2509.13732 (2025), arXiv:2509.13732 [astro-ph.HE].

[32] J. L. Friedman, J. R. Ipser, and R. D. Sorkin, *Astrophys. J.* **325**, 722 (1988).

[33] R. X. Xu, *The Astrophysical Journal* **596**, L59–L62 (2003).

[34] X. Y. Lai and R. X. Xu, *Monthly Notices of the Royal Astronomical Society: Letters* **398**, L31–L35 (2009).

[35] Y. Gao, X.-Y. Lai, L. Shao, and R.-X. Xu, *Monthly Notices of the Royal Astronomical Society* (2021), 10.1093/mnras/stab3181.

[36] H.-B. Li, Y. Gao, L. Shao, R.-X. Xu, and R. Xu, *Mon. Not. Roy. Astron. Soc.* **516**, 6172 (2022), arXiv:2206.09407 [gr-qc].

[37] C. Zhang, Y. Gao, C.-J. Xia, and R. Xu, *Physical Review D* **108** (2023), 10.1103/physrevd.108.063002.

[38] C. Zhang, Y. Gao, C.-J. Xia, and R. Xu, *Phys. Rev. D* **108**, 123031 (2023).

[39] W.-L. Yuan, C. Huang, C. Zhang, E. Zhou, and R. Xu, *Physical Review D* **111** (2025), 10.1103/physrevd.111.063033.

[40] S. A. Bludman and M. A. Ruderman, *Phys. Rev.* **170**, 1176 (1968).

[41] G. Caporaso and K. Brecher, *Phys. Rev. D* **20**, 1823 (1979).

[42] N. Stergioulas and J. L. Friedman, *The Astrophysical Journal* **444**, 306 (1995).

[43] A. Bauswein and N. Stergioulas, *Monthly Notices of the Royal Astronomical Society* **471**, 4956–4965 (2017).

[44] D. J. Reardon, M. Bailes, R. M. Shannon, C. Flynn, J. Askew, N. D. R. Bhat, Z.-C. Chen, M. Curylo, Y. Feng, G. B. Hobbs, A. Kapur, M. Kerr, X. Liu, R. N. Manchester, R. Mandow, S. Mishra, C. J. Russell, M. Shamohammadi, L. Zhang, and A. Zic, *The Astrophysical Journal Letters* **971**, L18 (2024).

[45] T. E. Riley, A. L. Watts, P. S. Ray, S. Bogdanov, S. Guillot, S. M. Morsink, A. V. Bilous, Z. Arzoumanian, D. Choudhury, J. S. Deneva, K. C. Gendreau, A. K. Harding, W. C. G. Ho, J. M. Lattimer, M. Loewenstein, R. M. Ludlam, C. B. Markwardt, T. Okajima, C. Prescod-Weinstein, R. A. Remillard, M. T. Wolff, E. Fonseca, H. T. Cromartie, M. Kerr, T. T. Pennucci, A. Parthasarathy, S. Ransom, I. Stairs, L. Guillemot, and I. Cognard, *The Astrophysical Journal Letters* **918**, L27 (2021).

[46] T. E. Riley, A. L. Watts, S. Bogdanov, P. S. Ray, R. M. Ludlam, S. Guillot, Z. Arzoumanian, C. L. Baker, A. V. Bilous, D. Chakrabarty, K. C. Gendreau, A. K. Harding, W. C. G. Ho, J. M. Lattimer, S. M. Morsink, and T. E. Strohmayer, *The Astrophysical Journal Letters* **887**, L21 (2019).

[47] S. Vinciguerra, T. Salmi, A. L. Watts, D. Choudhury, T. E. Riley, P. S. Ray, S. Bogdanov, Y. Kini, S. Guillot, D. Chakrabarty, W. C. G. Ho, D. Huppenkothen, S. M. Morsink, Z. Wadiasingh, and M. T. Wolff, *The Astrophysical Journal* **961**, 62 (2024).

[48] D. Choudhury, T. Salmi, S. Vinciguerra, T. E. Riley, Y. Kini, A. L. Watts, B. Dorsman, S. Bogdanov, S. Guillot, P. S. Ray, D. J. Reardon, R. A. Remillard, A. V. Bilous, D. Huppenkothen, J. M. Lattimer, N. Rutherford, Z. Arzoumanian, K. C. Gendreau, S. M. Morsink, and W. C. G. Ho, *The Astrophysical Journal Letters* **971**, L20 (2024).

[49] N. Rutherford, M. Mendes, I. Svensson, A. Schwenk, A. L. Watts, K. Hebeler, J. Keller, C. Prescod-Weinstein, D. Choudhury, G. Raaijmakers, T. Salmi, P. Timmerman, S. Vinciguerra, S. Guillot, and J. M. Lattimer, *The Astrophysical Journal Letters*

971, L19 (2024).

[50] R. Abbott *et al.*, *The Astrophysical Journal Letters* **896**, L44 (2020).

[51] K. Takami, L. Rezzolla, and S. Yoshida, *Monthly Notices of the Royal Astronomical Society: Letters* **416**, L1–L5 (2011).

[52] A. Tsokaros, M. Ruiz, L. Sun, S. L. Shapiro, and K. Uryū, *Physical Review Letters* **123** (2019), 10.1103/physrevlett.123.231103.

[53] A. Tsokaros, M. Ruiz, and S. L. Shapiro, *Physical Review D* **101** (2020), 10.1103/physrevd.101.064069.

[54] M. Ruiz, A. Tsokaros, S. L. Shapiro, K. C. Nelli, and S. Qunell, *Physical Review D* **102** (2020), 10.1103/physrevd.102.104022.

[55] E. Troja, H. van Eerten, B. Zhang, G. Ryan, L. Piro, R. Ricci, B. O’Connor, M. H. Wieringa, S. B. Cenko, and T. Sakamoto, *Mon. Not. Roy. Astron. Soc.* **498**, 5643 (2020), arXiv:2006.01150 [astro-ph.HE].

[56] Z. Li, Z. Chen, Y. Huang, Y. Lu, and J. Liu, *arXiv e-prints* , arXiv:2509.14124 (2025), arXiv:2509.14124 [astro-ph.HE].